

PACS numbers: 42.30.Ms; 42.30.Wb; 87.64.Cc
DOI: 10.1070/QE2008v038n06ABEH013867

Application of laser speckles for identification of tissues with pathological changes

A.S. Ulyanov

***Abstract*. Two new techniques for the analysis of speckle-patterns, formed by laser radiation dispersed on histological sections with malignant and non-malignant growths, are proposed. One of these techniques is based on the calculation of invariant Zernike moments of the spatial distribution of the speckle-field intensity. The second technique is based on the calculation of the fractal dimension of the intensity spatial distribution in the speckle structure. It is shown that both these methods yield the same results, which drastically depend on tissue properties. The possibility of using Zernike moments and fractal dimensions, formed by laser light dispersed on histological sections, in *in vitro* express-diagnostics of tissues with pathological changes is investigated.**

Keywords: *speckle-pattern, correlation function, Zernike moments, fractal dimension, cancerous growth.*

1. Introduction

For a long time speckle-fields have been used for analysis of characteristics of dispersive objects and the character of their motion [1]. In some cases, statistical characteristics of speckle-fields can be useful to obtain information about average dimensions of dispersive objects, the degree of roughness, etc. [1]. Speckle dynamics can be used to determine the displacement of moving dispersive objects, the degree of their deformation and the velocity of dispersive flows. In the biomedical optics, speckle-fields are widely used in optical diagnostics of biotissues [2], for measurements of the blood flow velocity [3] and investigation of the cerebrum microvascular topology [4, 5]. Note that statistical characteristics of speckle-fields slightly depend on characteristics of dispersive objects [6 – 8]. Developed speckles usually obey the Gaussian statistics [6], their size depends on the scattering configuration (emission wavelength, size of the illuminated object, distance between a dispersive object and observation plains), and the speckle contrast is equal to 1.

Nevertheless, not in all cases these statements are true. If the phase fluctuation caused by a dispersive object obeys the *K*-distribution, the speckle-field statistics should also obeys the *K*-distribution [9, 10]. As shown in Refs [11 – 14], if the object has some fractal features, the speckle-pattern formed by this object also can have fractal characteristics. There is a number of papers devoted to the so-called 'fractal speckles' (see paper [15] and references therein).

In biology, medicine and biophysics the fractal dimension analysis has recently found the application. There have been a few investigations devoted to the possibility of using fractal dimensions to describe characteristics of different biological objects. Thus, fractal dimensions have been used to select single healthy cells from cancerous cells by using the electron microscopy methods [16]. In review [17] fractal characteristics of the vascular topology of cerebrum pial membranes were described.

Invariant Zernike moments are widely used to describe structural image characteristics [18, 19]. But Zernike moments are rarely used in biology. As a matter of fact, there is only one paper [20] in which Zernike moments, calculated on the scattering indicatrix, were used to identify the degree of bacterial colonies' pathogenicity.

The aim of this paper is to study the possibility of using specific methods for digital speckle-pattern processing (calculation of the fractal dimension and Zernike moments) in express-diagnostics of tissues with pathological changes. The first attempt is made to use Zernike moments and fractal dimensions in digital speckle-pattern processing to identify biotissues with different new growths. It is shown that tissues with non-malignant growths form speckle-fields with fractal dimensions, which differ from speckle-patterns formed by tissues with malignant growths.

2. Methods and materials

A 1-mW, 633-nm HN-5P He – Ne laser has been used in experiments. A Gaussian laser beam with a diameter of 1 mm was transformed to a collimated beam with a diameter of 1 cm. The collimated beam was produced by using a system consisting of two lenses. The first lens with the focal distance 1.14 mm and numerical aperture 0.44 (C200TM-B, Thorlab, USA) focused the beam to a spot of diameter ~ 2 μm (the spot size was estimated using the equation for the Airy disc [7]). The front focal plane of the second lens with the focal distance of 10 mm and numerical aperture 0.55 (AL1210-A, S-LAH64 Aspheric Lens, Thorlab, USA) coincided with the back focal plane of the first lens. A spatial filter was placed [with a small pinhole of diameter 5 μm (P5S, Thorlab, USA)] in the plane of the focused beam. Both lenses and the spatial filter were

A.S. Ulyanov N.G. Chernyshevsky Saratov State University, ul Astrakhanskaya 83, 410012 Saratov, Russia; e-mail: UlyanovAS@mail.ru

Received 12 February 2008
Kvantovaya Elektronika **38** (6) 557 – 562 (2008)
Translated by A.S. Ulyanov

assembled in the standard optical tube (SM05L10, 0.5″ Lens Tube, Thorlab, USA). The collimated laser beam was directed to the object under study by using a mirror (ME05-M01, Gold, Thorlab, USA).

Speckle-patterns were recorded with a monochrome CMOS Phoenics USB Digital 1298-M camera (MuTech, USA) having a resolution of 1280×1024 pixels. The pixel size of the camera was 5.2 μm. In some cases of illumination, an IR filter can cause the appearance of slanted interference fringes in the detection plain. Because of this, the IR filter was removed from the camera.

The histological sections under study were prepared on freezing microtome in accordance with the standard technique and had a thickness of 200 ± 5 μm. The histological sections were fixed between the object and microscope cover glasses. The lateral dimension of objects was somewhat larger than the diameter d of the illuminating beam (i.e. $d = 1$ cm).

The distance z between the illuminated object and speckle detection plane (surface of the silicone area of the CMOS camera) was 14 cm. The average lateral dimension of speckles in the detection plane can be estimated by using the expression [21, 22]

$$a \approx \frac{3\lambda z}{d}. \tag{1}$$

Hence, in the case under study ($\lambda = 0.63$ μm, $z = 14$ cm, $d = 1$ cm), the estimated size of speckles was about 25 μm, which is 5 times larger than the pixel size of the CMOS camera.

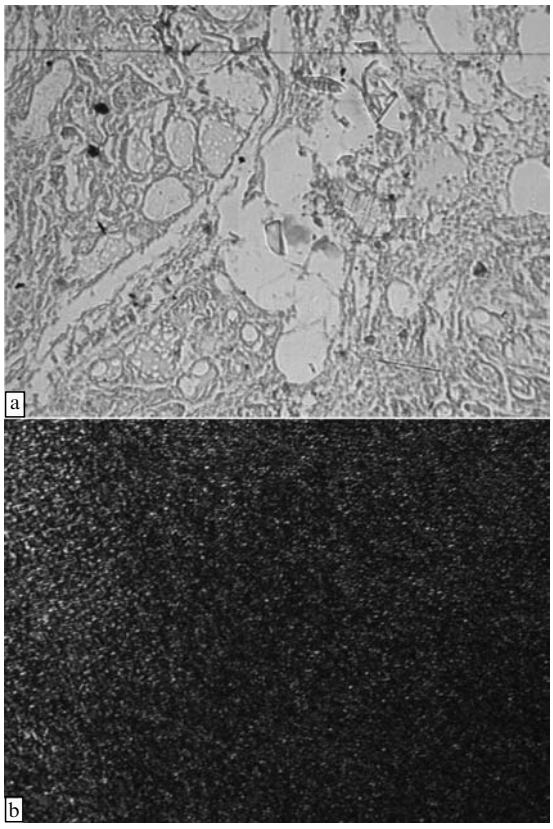

Figure 1. A non-malignant growth (a) and a speckle-pattern (b) corresponding to (a).

Figures 1b and 2b show typical speckle-patterns, formed by dispersive laser radiation on samples under study. The recorded images have, as a rule, an insignificant two-dimensional trend [23] (Fig. 3). This trend can be obtained by using the convolution of the Gaussian function with a two-dimensional image of the detected speckle-pattern (the width of the convolution window was 50×50 pixels). The intensity of recorded speckle-patterns in each point was normalised on the magnitude of the trend. In other words, the obtained trend was used to suppress large-scale fluctuations of the speckle-patterns intensity.

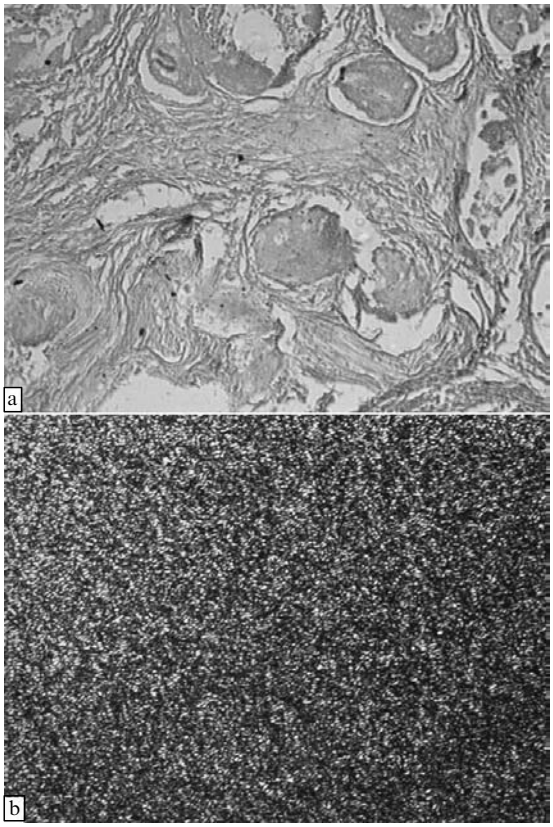

Figure 2. Malignant growth (a) and a speckle-pattern (b) corresponding to (a).

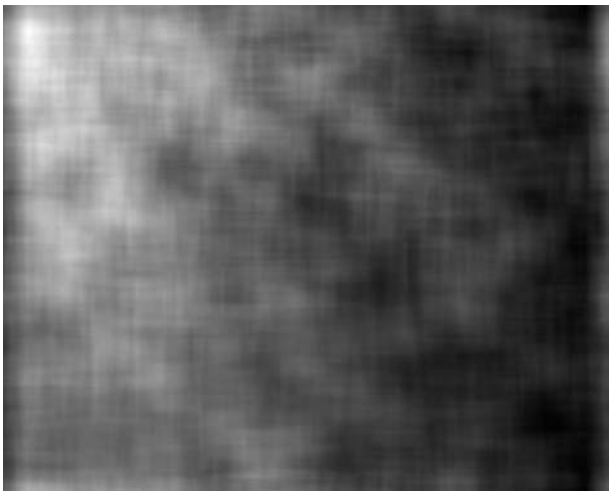

Figure 3. Two-dimensional trend, obtained from the speckle-pattern.

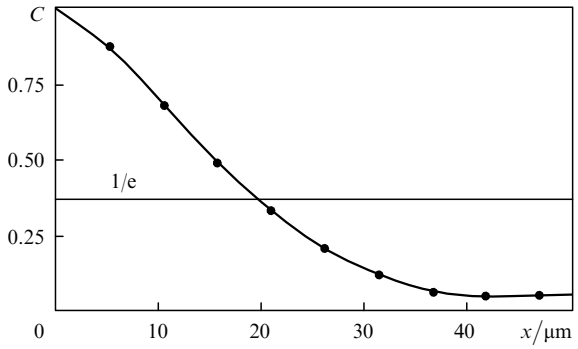

Figure 4. Autocorrelation function of intensity space fluctuations.

A typical example of the normalised one-dimensional autocorrelation function (coefficient of autocorrelation) is shown in Fig. 4. The central horizontal line of the speckle-pattern was used to calculate the autocorrelation function. One can see that the correlation length (20 μm) obtained in experiments is in good agreement with the theoretical estimate (25 μm), which was obtained by using (1).

Experiments show that the speckle-field, formed by laser radiation dispersed on histological sections, is completely depolarised on average and the speckle contrast (see Ref. [6]) is 0.67.

It is known [8] that the distribution function of the intensity probability density of multiply scattered light is described by the function [8]

$$p(I) = \left(\frac{2}{\langle I\rangle}\right)^2 I \exp\left(-\frac{2I}{\langle I\rangle}\right), \tag{2}$$

where $\langle I\rangle$ is the average intensity. The speckle contrast for the distribution described by Eqn (2) is equal to 0.7.

The histogram of intensity fluctuations obtained experimentally is shown in Fig. 5 (the sample size was 1.3×10^6, the number of intervals in the histogram was calculated by using the Sturgess expression [24]). The hypothesis about the type of the distribution has not tested in this work, but, one can see from Fig. 5 that speckle statistics obeys distribution (2) of depolarised thermal radiation.

Thus, the shape of the distribution function of the intensity probability density, the contrast speckle magnitude (about 0.7) and the changes in the polarisation structure of radiation, passed through the scattering object, indicate the regime of multiple scattering of light in histological sections.

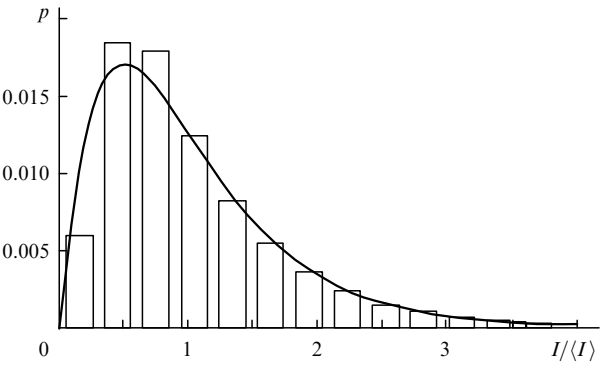

Figure 5. Histogram of intensity space fluctuations.

3. Methods for speckle-pattern analysis, based on calculation of Zernike moments and fractal dimensions

3.1 Zernike moments

Consider a two-dimensional continuous stochastic speckle-field intensity distribution $I(x, y)$.

The equation describing Zernike moments of the function $I(x, y)$ (see, for example, Refs [19, 20]) has the form:

$$A_{n,m} = \int\int I(x,y) V_{n,m}(x,y) \mathrm{d}x\mathrm{d}y. \tag{3}$$

Here, $V_{n,m}$ is a polynomial which depends on x and y in powers of n and m, and is described by:

$$V_{n,m}(x,y) = R_{n,m}(\rho)\mathrm{e}^{-\mathrm{i}m\theta}, \tag{4}$$

where $\rho = \sqrt{x^2+y^2}/\rho_0$; $\theta = \arctan(y/x)$; n is the non-negative integer; $|m|$ is the number less or equal to n, which satisfies $(n - |m|)$; ρ_0 is the radius of a circle, inscribed in the square field where the speckle-pattern is recorded;

$$R_{n,m}(\rho) = \sum_{s=0}^{(n-|m|)/2} (-1)^s \times \frac{(n-s)!\rho^{n-2s}}{s![(n+|m|-2s)/2][(n-|m|-2s)/2]} \tag{5}$$

is a radial polynomial
Taking into account the symmetry property:

$$R_{n,m}(\rho) = R_{n,-m}(\rho), \tag{6}$$

and using (3)–(5) for the continuous function, which describes the intensity in a two-dimensional speckle-structure, one can derive the final equation for Zernike moments

$$A_{n,m} = \frac{n+1}{\pi}\int_0^{2\pi}\int_0^1 I(\rho,\theta)R_{n,m}(\rho)\mathrm{e}^{-\mathrm{i}m\theta}\mathrm{d}\rho\mathrm{d}\theta. \tag{7}$$

Note that obtained moments are invariant to the image rotation. It means that if the image is rotated by an angle α:

$$I'(\rho,\theta) = I(\rho,\theta-\alpha). \tag{8}$$

Then, the equation of Zernike moments will be written in the form:

$$A'_{n,m} = \frac{n+1}{\pi}\int_0^{2\pi}\int_0^1 I(\rho,\theta-\alpha)R_{n,m}(\rho)\mathrm{e}^{-\mathrm{i}m\theta}\rho\mathrm{d}\rho\mathrm{d}\theta. \tag{9}$$

By introducing a new variable $\theta_1 = \theta - \alpha$, equation (9) will be written in the form:

$$A'_{n,m} = \left[\frac{n+1}{\pi}\int_0^{2\pi}\int_0^1 I(\rho,\theta_1)R_{n,m}(\rho) \times \mathrm{e}^{-\mathrm{i}m\theta_1}\rho\mathrm{d}\rho\mathrm{d}\theta_1\right]\mathrm{e}^{-\mathrm{i}m\alpha} = A_{n,m}\mathrm{e}^{-\mathrm{i}m\alpha}. \tag{10}$$

The above analysis shows that the argument of the Zernike moments changes upon rotation (orientation angle), but their magnitudes remain constant.

Note that in experiments the spatial distribution of the scattered light intensity (speckle-pattern) is recorded by CCD or CMOS cameras that allow the digital speckle-pattern to be processed. In this case, it is expedient to write the expression of Zernike moments in a discrete form. To introduce the discrete function, it is necessary to replace integrals in (7) by summations over the corresponding variables ρ_d and θ_d:

$$A_{n,m} = \frac{n+1}{\pi} \sum_{\rho_d} \sum_{\theta_d} I(\rho_d, \theta_d) R_{n,m}(\rho_d) e^{-im\theta_d}. \quad (11)$$

It was shown in [20] that Zernike moments of the discrete image also are invariant to the image rotation.

Note that characteristics such as Tchebyshev moments and Legendre polynomials are often used to characterise image properties (see Refs [25, 26]). But these characteristics are not invariant to the image rotation. It is important to stress that the invariant property is very useful in real situations because the speckle-pattern is determined by the object structure and its orientation in space. In experiments it is impossible to prepare histological sections that would be identically orientated in space. Even the absolutely identical objects, prepared from the same biotissue of the same patient, would be rotated randomly relative to each other. Orientation of two different objects, prepared from biotissues of different patients would be absolutely random, even if the objects are identical in the statistical sense. Thus, if statistical characteristics of speckle-fields, formed by scattering from the object under study, depend randomly on its location, these characteristics also will have random properties. In other words, statistical characteristics of speckle-patterns which are non-invariant to rotation (such as Tchebyshev moments or Legendre polynomials) are absolutely non-informative and cannot be used in diagnostics of biotissues.

3.2 Fractal dimensions

Last few years apart from conventional methods (such as the distribution function of the intensity fluctuation probability density, the correlation function and correlation moments of higher orders) [27], fractal dimensions have been used to describe the properties of speckle-patterns [15]. The calculation procedure of fractal dimensions consists of several steps. The first step is to obtain an average intensity magnitude $\langle I \rangle$ of the image under study. Then, the initial image is transformed into a new binary (black-and-white) image. The transformation should satisfy the following rule: if the intensity of the original image is higher than $\langle I \rangle$, the magnitude of this point equates to the maximum magnitude. If this rule is not fulfilled, the point magnitude equates to zero.

The next step is to cover the new binary image by boxes with the cell size ε and to calculate the number $N(\varepsilon)$ of cells covering the object under study. The lesser the cell size ε, the bigger the number of covering cells $N(\varepsilon)$ (see Figs 6a,b). As a result, the fractal dimension of the object [28] has the form

$$D = -\lim_{\varepsilon \to 0} \frac{\lg N(\varepsilon)}{\lg \varepsilon}. \quad (12)$$

Because the interval of self-similarity of a biological object is limited, the cell size can vary only in a certain range, whose maximum size is determined by the size of the image, and the minimum – by a minimal structure element (in the case of a digital image it is the pixel size). Thus, in our case expression (12) is useless and the fractal dimension should be calculated by using interpolation. This interpolation consists in obtaining the dependence of the number of covering cells on the cell size (in log–log plot) and revelation of a linear section of the dependence [28]. The slope angle of this linear section allows one to estimate the value of the fractal dimension.

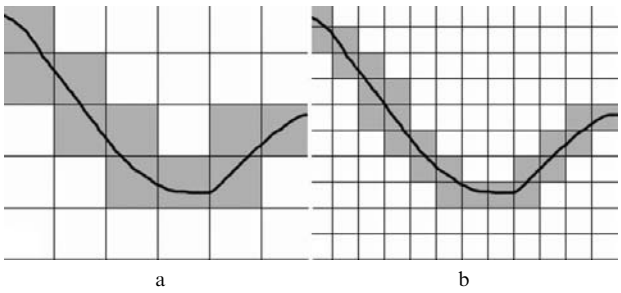

Figure 6. Fractal dimension calculation procedure (a – cells covering line are filled with grey; b – cell size was decreased, cells covering line are filled with grey).

4. Discussion

Figures 1a and 2a show histological sections with different types of growths: non-malignant (Fig. 1a) and malignant (Fig. 2a). Images have been obtained by the transmission light microscope with a microscope objective having the magnification $40^{\times}$. The CMOS camera was placed in the microscope image plane. Dimensions of the CMOS camera were 5×7 mm. Due to this circumstance, the linear sizes of the histological sections were 125×175 μm. Figures 1b and 2b show speckle-patterns, formed by illuminating histological sections.

Note that there is no visual difference between Figs 1b and 2b. The correlation analysis is also useless to obtain differences between them. The contrast of speckles and their average size, the shape of intensity fluctuation histograms and correlation functions are the same and are within the limits of the statistical sample error.

Invariant Zernike moments show the difference between speckle-patterns. Despite the fact that it is difficult to locate great differences between objects prepared from tissues with malignant and non-malignant growths, the magnitudes of calculated moments can differ from each other to one by an order and a half. It is difficult to propose a well-founded physical description of the observed effects now. Nevertheless, experimental results show that the magnitude of Zernike moments corresponding to malignant growths (modulus of the complex number $A_{n,m}$) is higher than the magnitude of moments corresponding to non-malignant growths.

Figure 7 shows data obtained for a small sampling. Speckle-patterns obtained by illuminating 29 histological sections, which corresponded to tissues with non-malignant (14 objects) and malignant (15 objects) growths, were analysed. The type of the growth was determined by using histological techniques.

The results of the empirical analysis show that there is a level of amplitudes of second order moments. Above this

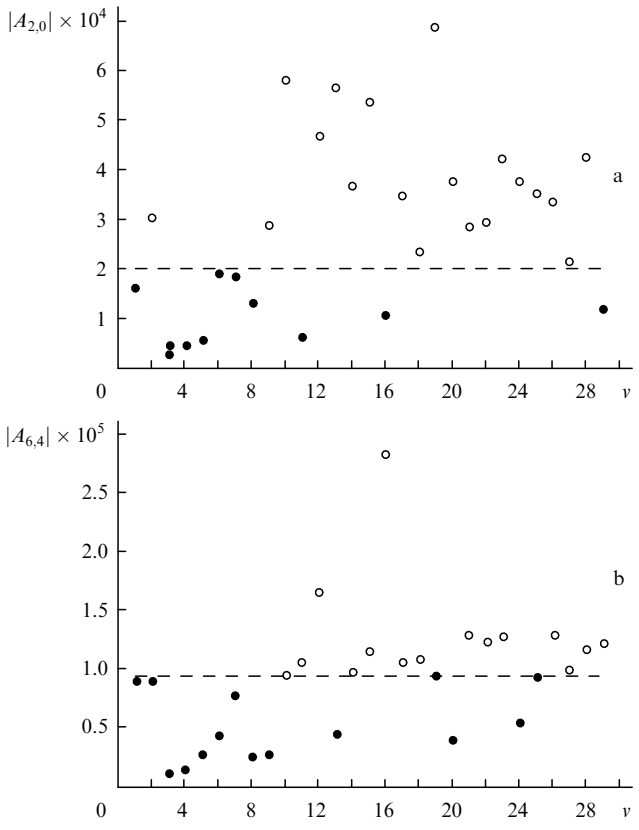

Figure 7. Maximum of magnitudes of Zernike moments with $n = 2$ and $m = 0$ (a) and with $n = 6$ and $m = 4$ (b), where $|A_{n,m}|$ is the moment modulus and v is the number of the object under study.(○) – malignant growth and (●) – non-malignant growth.

level, points corresponding to the malignant growth are located and below this level, points corresponding to the non-malignant growth are located. This feature is valid for moments of the order higher than 2 (Fig. 7b).

Figure 8 shows log – log plots determining fractal dimensions (Figs 8a, c) and the dependence of the increment of the logarithmic magnitude of the number of covering cells on the logarithmic magnitude of their size (Figs 8b, d). The linear section in Figs 8a, c corresponds to cell sizes when the fractal structure can be observed. Note that the dependence of the increment of the logarithmic magnitude of the number of covering cells is more informative, because the observation region of the fractal structure (taking into account the error, the increment in this region should be the same) can be detected more precisely.

There are two regimes of the fractal dimension behaviour: smooth and jumpwise augmentation of the increment. The smooth regime corresponds to tissues with malignant growths and the jumpwise regime – to tissues with non-malignant growths.

5. Conclusions

It has been shown that the results obtained by using the fractal dimension analysis are in good agreement with the results obtained by using the Zernike moments analysis. Results of application of both these techniques depend on the type of pathological changes in tissues.

Note that the obtained results are only preliminary. The reliability of these results, from the diagnostics point of view, can be determined only by comparing wealthy tissues and tissues with pathological changes. Tissues with different changes have been compared in this work (malignant and non-malignant growths). It is clear that changes in malignant and non-malignant tissues can be similar to each other. Unfortunately, the comparison of speckle-patterns, formed by pathologically changed tissues, with speckle-fields, formed by wealthy tissues, is impossible. All histological sections can be prepared only from postoperative materials, which is done in this work or from cadaveric tissues (it is known that optical properties differ greatly from normal tissues).

Nevertheless, it has been shown that there is a principal possibility of using the above techniques for digital processing of speckle-patterns in express diagnostics, which may be an alternative to traditional histological methods. The techniques described in this paper are very important for

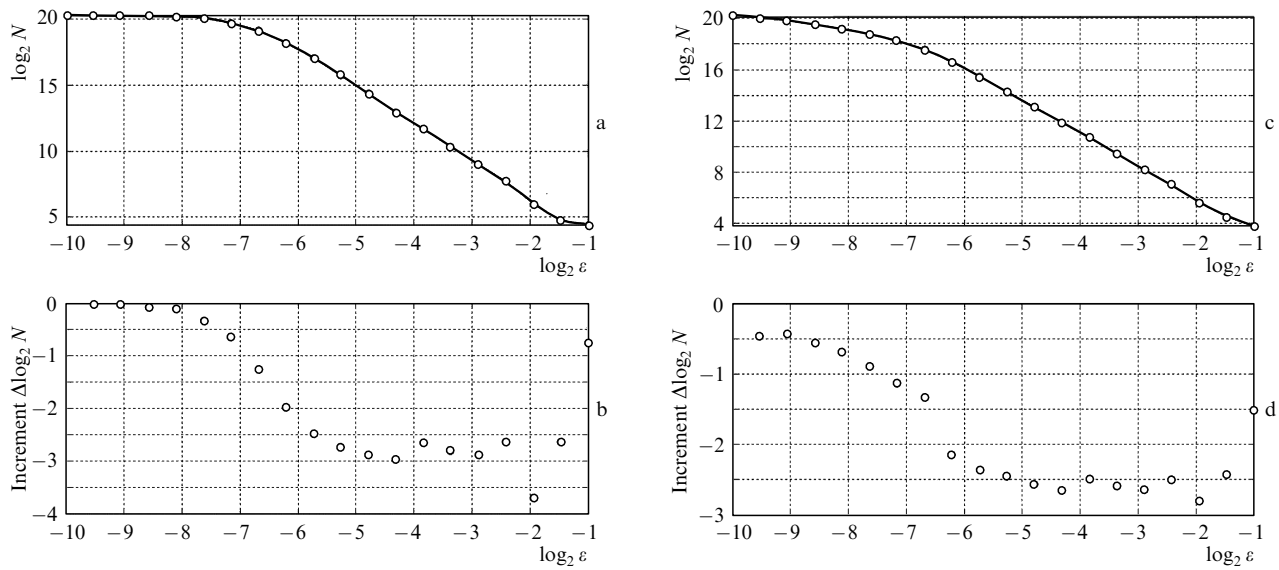

Figure 8. Dependences describing the fractal dimension of a malignant growth (a, b) and a non-malignant growth (c, d).

different applications because the traditional histological methods are very laborious and need well-qualified personnel.

Acknowledgements. This work was supported by the Russian Foundation for Basic Research (Grant Nos NNSF-a-06-04-39016, 07-02-01434 and RNP.2.1.1.4473). The author thanks G.S. Terentyuk for materials granted, A.A. Koronovskii and Yu.P. Volkov for consulting on fractal dimension analysis and I.L. Maksimova for fruitful discussions of the problem and obtained results.

References

1. Franson M. *La granularite laser (spekle) et ses applications en optique* (Paris: Masson, 1978).
2. Tuchin V.V. *Lasery i volokonnaya optika v biomedetsinskikh issledovaniyakh* (Lasers and Fibre Optics in Biomedical Investigations) (Saratov: Saratov State University Publishing House, 1998).
3. Galanzha E.I., Brill G.E., Aizu Y., Ulyanov S.S., Tuchin V.V., in *Handbook of Optical Biomedical Diagnostics* (Bellingham: SPIE Press Monograph, 2002).
4. Dunn A.K., Bolay H., Moskowitz M.A., Boas D.A. *J. Cerebral Blood Flow Metabolism*, **21**, 195 (2001).
5. Briers J.D., Webster S. *J. Biomed. Opt*., **1** (2), 174 (1996).
6. Dainty J.C. *Top. Appl. Phys.,* **9** (1975).
7. Goodman J.W. *Introduction in Fourier Optics* (San Francisco: Mcgraw-Hill Book Company, 1968).
8. Goodman J.W. *Statistical Optics* (New York: John Wiley & Sons Inc., 1985).
9. O'Donnell K.A. *J. Opt. Soc. Am*., **72**, 1459 (1982).
10. Newman D. *J. Opt. Soc. Am*., **2**, 22 (1985).
11. Ishii K., Asakura T. *J. Biomed. Opt*., **4** (2), 230 (1999).
12. Dogariu A., Uozumi J., Asakura T. *Waves in Random Media*, **4**, 1 (1994).
13. Dogariu A., Uozumi J., Asakura T. *Waves in Random Media*, **2**, 259 (1992).
14. Wada N., Uozumi J., Asakura T. *Pure Appl. Opt*., **4**, 857 (1995).
15. Funamizu H., Uozumi J. *Opt. Express*, **15** (12), 7415 (2007).
16. Bauer W., Mackenzie C.D. http://arxiv.org/pdf/patt-sol/9506003.pdf.
17. Eke A., Herman P., Kocsis L., Kozak L.R. *Physiol. Meas*., **23**, R1 (2002).
18. Liao S.X., Pawlak M. *IEEE Trans. on Pattern Analysis and Machine Intelligence*, **20** (12), 1358 (1998).
19. Khotanzad A., Hong Y.H. *IEEE Trans. on Pattern Analysis and Machine Intelligence*, **12** (5), 489 (1990).
20. Bayraktar B., Banada P.P., Hirleman D.E., Bhunia A.K., Robinson J.P., Rajwa B. *J. Biomed. Opt*., **11** (5) 034006-1 (2006).
21. Ryabukho V.P. *Soros Educational Journal*, **7** (5), 102 (2001).
22. Vest Ch.M. *Holographic Interferometry* (New York: John Wiley & Sons Inc., 1979).
23. Bendat J.S., Piersol A.G. *Random Data Analysis and Measurement Procedures* (New York: John Wiley & Sons Inc., 1986).
24. Stevens L. *Applied Multivariate Statistics for the Social Sciences*, (Hillsdale, New Jersey: Lawrence Erlbaum Associates Publishers, 1986).
25. Yap P.T., Raveendran P. *IEE Proc.–Vis. Image Signal Process*, **151** (2), 128 (2004).
26. Mukundan R., Ramakrishnan K.R. *Pattern Recognition*, **28** (9), 1433 (1995).
27. Zimnyakov D.A. *Opt. Eng*., **36** (5), 1443 (1997).
28. Ivanov A.V., Koronovskii A.A., Minyuhin I.M., Yashkov I.A. *Nonlinear Dynamics Afoot*, **14** (2), 64 (2006).